Chaos

Transport of blood particles: Chaotic advection even in a healthy scenario

Cite as: Chaos **30**, 093135 (2020); https://doi.org/10.1063/5.0013460
Submitted: 12 May 2020 . Accepted: 31 August 2020 . Published Online: 21 September 2020

I. M. Silva, A. B. Schelin, R. L. Viana, and I. L. Caldas

Chaos ARTICLE scitation.org/journal/cha

Transport of blood particles: Chaotic advection even in a healthy scenario

Cite as: Chaos **30**, 093135 (2020); doi: 10.1063/5.0013460
Submitted: 12 May 2020 · Accepted: 31 August 2020 ·
Published Online: 21 September 2020

I. M. Silva,[1] A. B. Schelin,[1,a)] R. L. Viana,[2] and I. L. Caldas[3]

AFFILIATIONS

[1]Instituto de Física, Universidade de Brasília, Campus Universitário Darcy Ribeiro, 70910-900 Brasília, Distrito Federal, Brazil
[2]Departamento de Física, Universidade Federal do Paraná, 81531-990 Curitiba, Paraná, Brazil
[3]Instituto de Física, Universidade de São Paulo, Rua do Matão, 1371, 05508-090 São Paulo, SP, Brazil

[a)]**Author to whom correspondence should be addressed:** schelin@unb.br

ABSTRACT

We study the advection of blood particles in the carotid bifurcation, a site that is prone to plaque development. Previously, it has been shown that chaotic advection can take place in blood flows with diseases. Here, we show that even in a healthy scenario, chaotic advection can take place. To understand how the particle dynamics is affected by the emergence and growth of a plaque, we study the carotid bifurcation in three cases: a healthy bifurcation, a bifurcation with a mild stenosis, and the another with a severe stenosis. The result is non-intuitive: there is less chaos for the mild stenosis case even when compared to the healthy, non-stenosed, bifurcation. This happens because the partial obstruction of the mild stenosis generates a symmetry in the flow that does not exist for the healthy condition. For the severe stenosis, there is more irregular motion and more particle trapping as expected.

In this work, we study the advection of blood particles in arteries with bifurcations. Such sites are typically affected by cardiovascular diseases that can lead to strokes, one of the main causes of death in the world. We focus on the carotid artery bifurcation. The role of the carotid artery is to supply the oxygenated blood to the brain. In the vessels configuration, a bifurcation splits the main carotid artery into the internal carotid artery and the external carotid artery. Over time, this anatomical region is prone to plaque formation. These plaques, composed typically by fatty substances and cholesterol deposits, create a local narrowing of the vase, increasing flow disturbance. Previous works show that chaotic advection of blood particles can often occur in blood vessels with diseases. Indeed, two basic ingredients are commonly found in the circulatory system: flow disturbance and time dependence. Here, we show that chaotic advection can occur even in healthy conditions. In such cases, the flow disturbance is naturally created by the bifurcation. As a result, chaotic advection of particles can initiate and aggravate cardiovascular diseases by trapping particles and increasing their probability of aggregation and attachment to the vessels wall. We study the carotid bifurcation in three different scenarios: the first case can be considered a normal and healthy bifurcation, while the other two are affected by plaques in the internal carotid artery. We show that in all scenarios, there is chaotic advection. Our results can explain why the carotid bifurcation is susceptible to atherosclerosis development.

I. INTRODUCTION

Atherosclerosis is the narrowing of the internal part of an artery as a result of a plaque build up. The disease is the main cause of natural death in developed countries.[1] Due to geometric characteristics, some arteries, such as the carotid and the coronary, are more prone to develop flow disturbance. Indeed, several works show that large variations of shear regions and fast oscillatory flows are responsible for the biochemical activation that initiates and sustains the plaque formation.[2–6]

Blood flows have a pulsatile nature due to the cardiac cycle.[3] This cycle is typically divided into two parts: the systole, when the heart contracts and pumps blood to the arteries, and the diastole, when the heart relaxes and is refilled with blood.

For time-dependent flows, recirculating zones can appear and, even though most of the vortices are washed away periodically, particles carried by such flows can become permanently trapped. In

fact, for unsteady flows, particle trajectories and streamlines are generally different. This is why the behavior of advected particles can become irregular and chaotic even in laminar flows. Indeed, blood flows in the circulatory system create the perfect environment for the appearance of chaotic advection.

Chaotic advection is the emergence of chaos in the transport of particles carried by flows.[7] Examples of applications include mixing devices,[8] biochemically active systems,[9] environmental flows,[10,11] and evolutionary models,[12] to cite a few.

For open flow systems, the manifestation of chaos is due to the presence of a chaotic set in a closed region of interest, the *mixing region*.[13] This set is called the *chaotic saddle* and is formed by infinite points of periodic and aperiodic orbits that never leave the mixing region. Mathematically, the chaotic saddle has a stable manifold, a set containing points that approach the chaotic saddle for $t \to \infty$, and an unstable manifold, a set formed by points that approach the saddle for $t \to -\infty$.

A distinctive characteristic of flows with chaotic advection is that one can physically visualize the unstable manifold of the system.[14] For example, let there be a blob of dye in a time-dependent flow. As time passes, this blob will deform, stretching and folding in a way that will result in a filamentary distribution of the dye. These filaments trace out the unstable manifold. This distribution of the dye has important consequences. For active systems, such as blood flows, where the advected quantities interact with each other in some way, the effects include high reactions rates and trapping zones. Indeed, the filaments act as a fractal catalyst for the system, for a review see Tel *et al.*[15]

Such a phenomenon is typical for two-dimensional incompressible flows. Consider, for example, the velocity field $\mathbf{u} = (u_x, u_y)$ with $\div\mathbf{u} = \partial u_x/\partial x + \partial u_y/\partial y = 0$ due to incompressibility. There exists a stream function $\psi(x, y, t)$ such that

$$\dot{x} = -\frac{\partial \psi}{\partial y}, \quad \dot{y} = \frac{\partial \psi}{\partial x}, \tag{1}$$

where $\mathbf{r} = (x, y)$ is the position of the advected particle.

Here, we identify a Hamiltonian structure of a one-degree-of-freedom system, where the phase-space corresponds to the physical plane of the flow. When the flow is time-dependent, the system behaves as a non-integrable time-depedent Hamiltonian. Therefore, typical structures from Hamiltonian chaos are directly visible in the flow. This dynamics is called *Lagrangian chaos*. In contrast with the well known fluid dynamics turbulence, Lagrangian chaos can take place even in laminar, periodic flows such as the ones found in blood vessels.

Previous works show that common cardiovascular diseases, such as stenosis and aneurysm, can generate chaotic advection of blood particles.[16–18] It was shown that more severe stenosis generate higher Lyapunov exponents.[16] In a more realistic model, Závodszky *et al.* model the blood flow in a realistic 3D cerebral aneurysm and show fractal patterns of tracers.[19]

It is important to mention that chaos in blood flows is a topic well studied in the context of Lagrangian Coherent Structures (LCSs).[5,20–23] Shadden *et al.*[24] introduced LCS as a new tool to characterize blood flows in large vessels. They showed that LCS can be used to identify several features of the flow, such as flow stagnation and separation. In particular, a 3D model of the carotid bifurcation was used and filamentary patterns of long residence time were traced. Arzani *et al.*[22] used a Lagrangian description to quantify wall shear stress exposure time, a quantity that is important in the context of platelet activation.

Here, we will show that even in healthy conditions, blood particles present chaotic dynamics. In this case, the bifurcation acts as a perturbation, generating flow structures that appear and disappear periodically. We also study the carotid bifurcation with two degrees of stenosis in the internal carotid artery: the mild case and the severe case. We show that there is less chaos, characterized by a lower fractal dimension of the stable manifold, for the mild case even when compared to the healthy carotid bifurcation. Indeed, this non-intuitive result is due to the symmetry that the partially obstructed carotid branch creates in the flow. For the severe stenosis, the fractal dimension is higher and particle trapping increases as expected.

This paper is divided as follows: in Sec. II, we show the methods used to simulate the blood flow and particle dynamics. Section III shows the results. We show the conclusions in Sec. IV.

II. METHODS

The modeling of the system includes three parts: (i) geometric model generation and boundary condition definitions, (ii) numerical simulations of the flow, and (iii) numerical simulation of particle tracing.

A simplified 2D model of the carotid was built with AUTOCAD, shown in Fig. 1. The geometry simulates a normal and healthy artery system.[6,25–27] We choose to work with a simple 2D model in order to give a better insight into the structure of the chaotic advection. After the bifurcation, the lower branch corresponds to the external carotid artery (ECA), while the upper one corresponds to the internal carotid artery (ICA). Typically, the ICA is more affected by plaques than the ECA. Such a site is also potentially more dangerous, since it is in the route taken by the oxygenated blood to the brain.

We consider three scenarios: (i) the healthy carotid bifurcation, case C1; (ii) the mild case, case C2, where the ICA is stenosed with a 56% occlusion; (iii) the severe case, case C3, where the ICA has a 82% occlusion. For more details about the geometric classification of the stenosis, see the Appendix.

For the boundary conditions, we imposed a periodic velocity following, at the inlet, the profile shown in Fig. 2.[6] There are two outlets, corresponding to the end of the two branches, where the pressure was fixed at 13 300 Pa.

The exact pattern of blood flows is hard to simulate since the geometry of the vessel varies for each individual Regarding this, we also tested different boundary conditions, such as different pressure patterns and velocities inlets and the qualitative results remain the same. For a more realistic 3D model of the carotid bifurcation, see Ref. 24.

Blood was considered to be Newtonian and incompressible, with $\rho = 1.06\,\mathrm{g/cm^3}$ and $\mu = 0.04\,\mathrm{g/cm\,s}$.

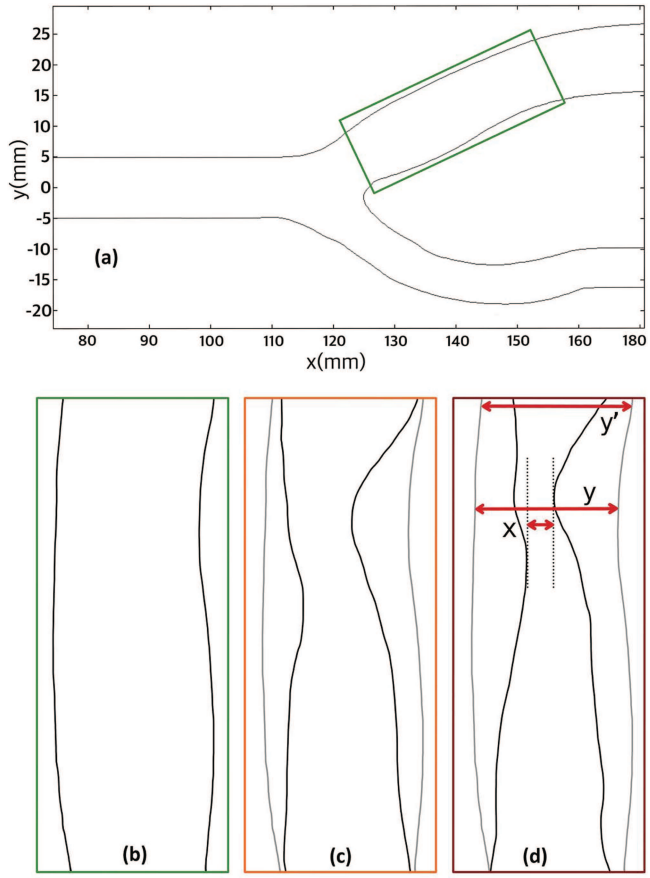

FIG. 1. (a) Geometry of the carotid artery bifurcation. Enlargement of the affected region for three different cases: (b) case C1, where the bifurcation is healthy, (c) case C2, where the ICA is obstructed by a mild stenosis, and (d) case C3, where the ICA is obstructed by a severe stenosis. Here, x is the vertical space between the occlusions, y is the total carotid wall thickness inside the stenosis region, and y' is the carotid diameter after the stenosis.

For the particle tracing, we considered massless particles, i.e. particles with size zero that follow the flow without inertia by

$$\frac{d\mathbf{r}(t)}{dt} = \mathbf{u}(\mathbf{r}, t), \tag{2}$$

where $\mathbf{r}(t)$ is the particles position and $\mathbf{u}(\mathbf{r}, t)$ is the flow velocity at position $\mathbf{r}$ and time t, obtained by the Navier–Stokes equations.

The Navier–Stokes equations were solved with the finite element software COMSOL.[28] The finer physics-controlled mesh of COMSOL with around 16×10^3 elements for each case. Error tolerance was defined as 1×10^{-4} and relative tolerance was fixed at 0.01. For time stepping, the generalized alpha method was used with a maximum time step of 0.01 s. For a video tutorial, see the supplementary material.

Ten cardiac cycles were simulated and the last seven were used for analysis. We now show the results for the particle advection in each scenario.

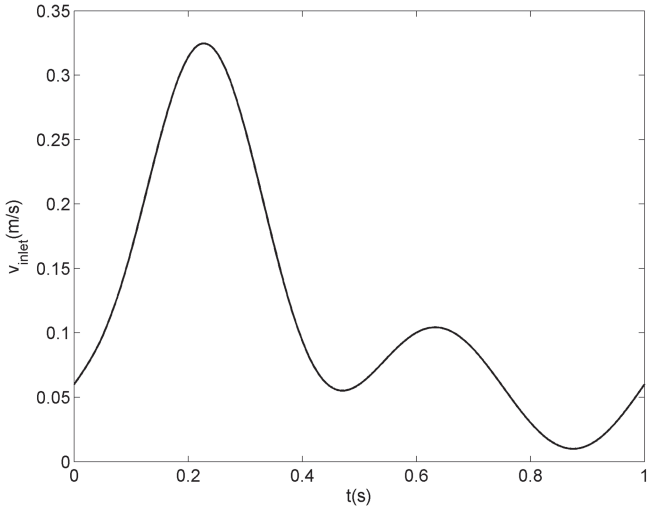

FIG. 2. Inlet velocity of the flow in m/s for one cardiac cycle.

III. RESULTS

A. Time decay

Flow disturbances commonly generate coherent structures, such as vortices, that typically trap advected particles, increasing their residence time in the observation region. This has shown to be true for blood flows in Refs. 16, 20, 21, and 24 and is also verified here for the carotid bifurcation. The main difference for this case, however, is that we have to take into account through which exit the particle leaves.

Figure 3 shows three semi-log graphics of the number of particles inside the observation region vs time. To perform the calculation, a line of 10^4 particles was released from upstream ($x = 100$ mm) at four different time-phases of the cardiac cycle ($t = 0$, $t = 1/4T$, $t = 1/2T$, $t = 3/4T$) and the time they spent before exiting was calculated. We then calculated the mean residence time for each initial condition considering the four releases.

In Fig. 3(a), we show the mean residence time for all particles independently of their exit. We see that the behavior is similar for all three cases, with a faster particle decay for the mild stenosis.

If we consider only the particles that leave through the stenosed branch (ICA), the situation changes. In Fig. 3(b), we find that for the severe obstruction, particles spend up to one cardiac cycle more trapped than particles of the healthy scenario in the observation region.

Now, we look at particles exiting the non-stenosed branch (the ECA), shown in Fig. 3(c). For this exit, particles take more time to leave in the healthy case as compared to the diseased bifurcations.

B. Stable manifolds

As the particles are carried by the flow, some leave the bifurcation region very fast while others spend more time at the observation site. To understand how this distribution takes place, we now calculate the stable manifold of the chaotic saddle for each case.

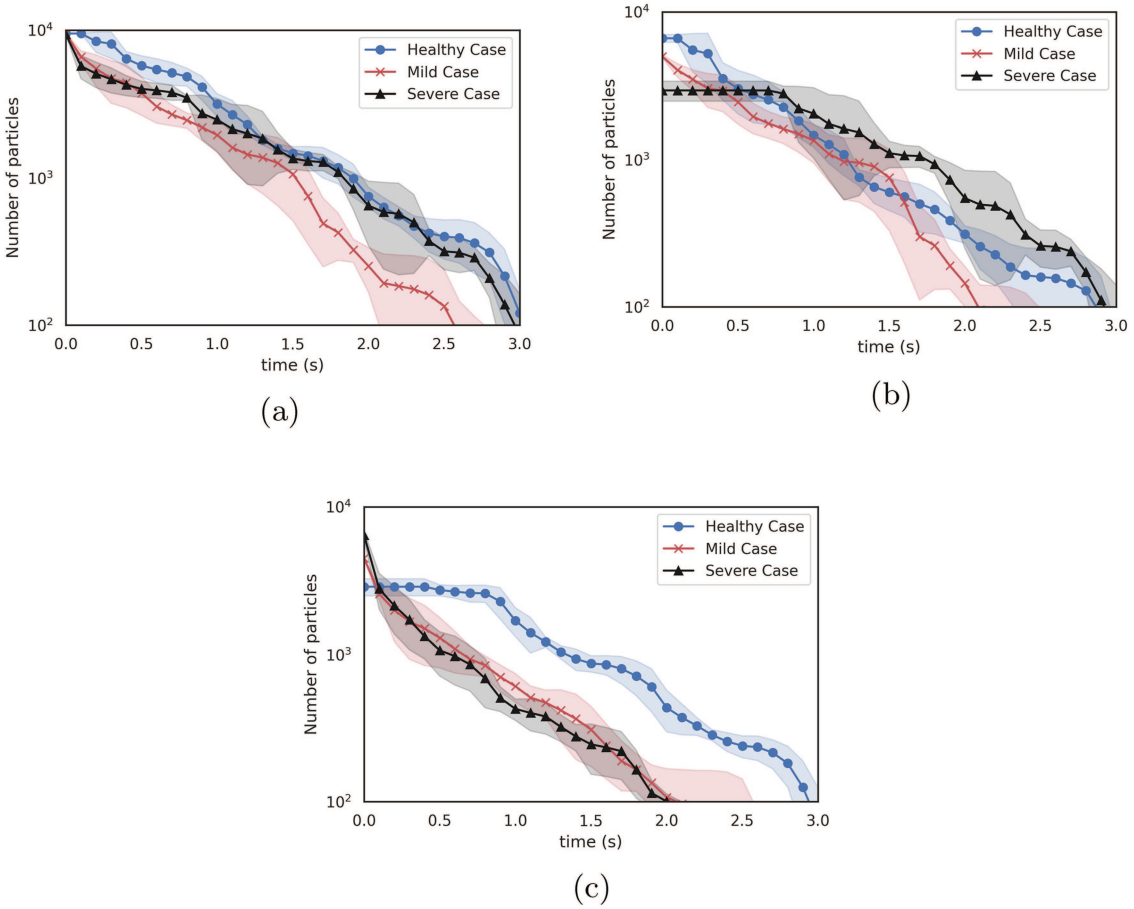

FIG. 3. Mean number of particles vs time considering four different time-phases of the cardiac cycle ($t = 0$, $t = 1/4T$, $t = 1/2T$, $t = 3/4T$). (a) Particles that leave in either of the two exits, (b) particles that leave through the ICA (the stenosed branch), (c) particles that leave through the ECA (healthy branch). The blue line corresponds to the healthy case C1, while the red line corresponds to the mild case C2 and the black line, the severe case C3.

An approximation of the stable manifold of the chaotic saddle was obtained by the sprinkler method.[29,30] The procedure consists of taking a grid of 400 × 400 initial conditions that cover the carotid bifurcation and the stenosed area at $t = 1/2T$. The trajectory of each initial condition is calculated, and the initial points of particles that spend more time wandering around the observation region are then colored in black.

As shown in Fig. 4(a), we see that for the healthy scenario there are several filaments that distribute themselves after the bifurcation in both branches. Indeed, these filaments indicate that there is chaotic advection even in the absence of a disease. These filaments appear to be fractal structures, a signature of chaos in flows.

The results are shown in Table I. The dark regions that appear before the bifurcation, close to the vessels wall, are mainly due to the no-slip boundary condition imposed as a boundary condition for the flow.

For the mild stenosis, shown in Fig. 4(b), we see that there are more filaments in the diseased branch, the ICA, although small filaments are still visible in the ECA. We also identify a barrier in the middle of the common carotid, the artery before the bifurcation, separating the upper part of the flow from the lower one.

As the stenosis aggravates, we see in the severe case, shown in Fig. 4(c), that all the filaments accumulate at the ICA branch, while the ECA remains clear. Indeed, this asymmetry is due to the flow behavior: with the ICA mostly blocked, the blood flow leaves the bifurcation region as a jet through the ECA, rapidly washing away the particles at this site.

We measured the fractal dimension of the filaments of the stable manifolds for each case using the box-counting method. The

TABLE I. Fractal dimension of the stable manifolds.

	C1	C2	C3
D	1.65 ± 0.03	1.46 ± 0.04	1.75 ± 0.04

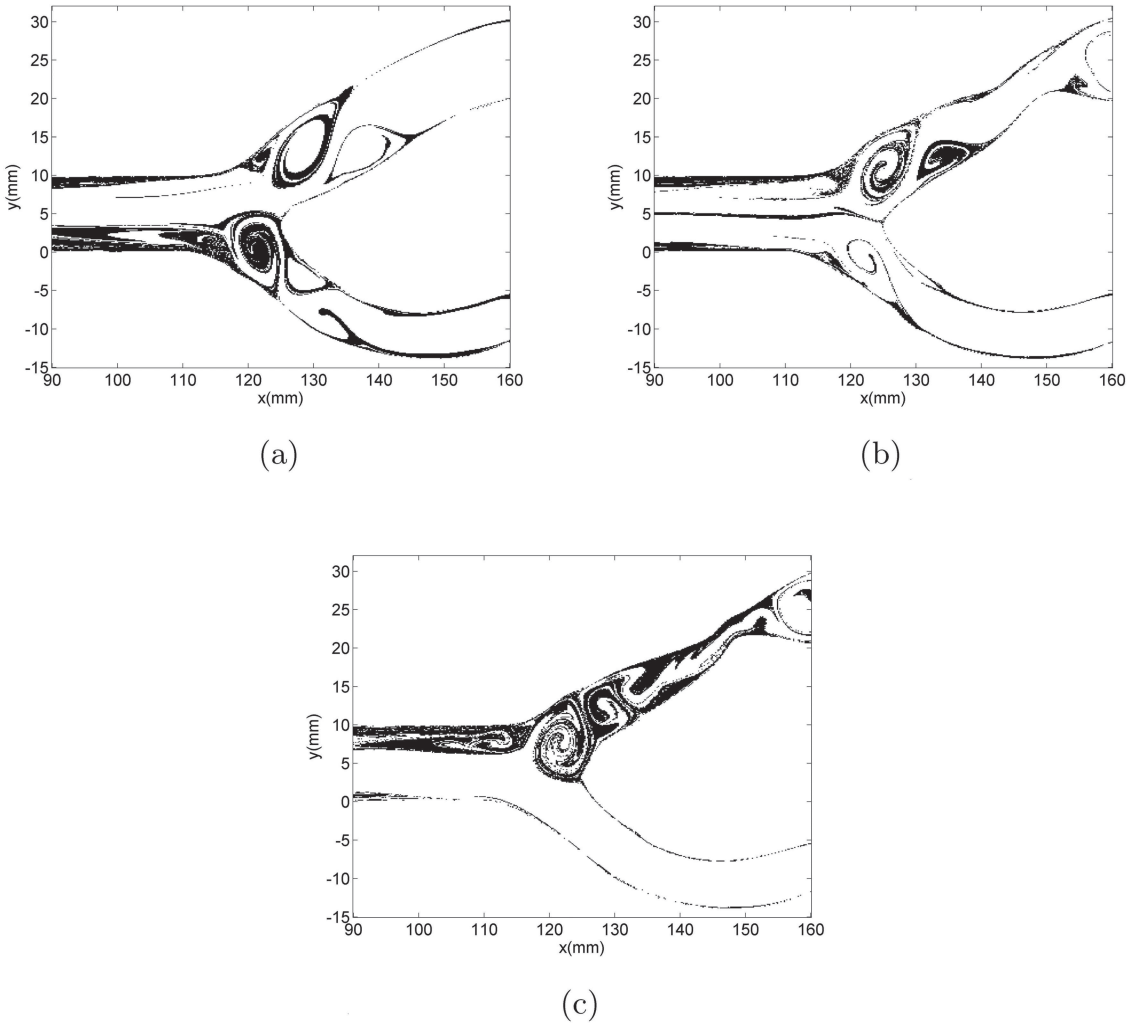

FIG. 4. Snapshot of the stable manifold for each case at $t = 1/2T$. (a) Healthy case C1. (b) Mild stenosis C2. (c) Severe stenosis C3.

box-counting method is a well known technique to estimate the fractal dimension of a dataset. The procedure consists of repeatedly covering the fractal filaments with a grid, each time with smaller boxes. The number of boxes N that cover the fractal set should scale with the size of the box ϵ as

$$D = \frac{\ln N(\epsilon)}{\ln 1/\epsilon} \lim_{\varepsilon \to 0}. \tag{3}$$

The fractal dimension corresponds to the slope of the line given by $\ln N$ and $\ln \epsilon$. For more details, see Ref. 31.

The results are shown in Table I. For the healthy case, the fractal dimension found is around 1.65. For the mild stenosis this value decreases, with $D = 1.46$, and for the severe stenosis it increases again with $D = 1.75$. From this result, we can conclude that there is "less chaos" in the mild scenario. This is due to the symmetry in the mass flow induced by the partial obstruction in the ICA. Indeed, this symmetry generates the barrier mentioned previously.

Typically, the shape of the filaments change periodically with the flow, the fractal distribution though shall remain the same. This fractal distribution plays an important role in systems where particles react with each other. It has been shown that the production term can be modeled by Ref. 15:

$$P c^{-\gamma} \tag{4}$$

where c is the concentration of the active particles and γ is given by $\gamma = (D-1)/(2-D)$. Therefore, the information of a changing, non-monotonic, fractal dimension as the size of the plaque changes must be taken into account.

The stable manifold does not tells us through which branch each particle is leaving. For instance, initial points that belong to filaments in the lower branch can leave the bifurcation site through the

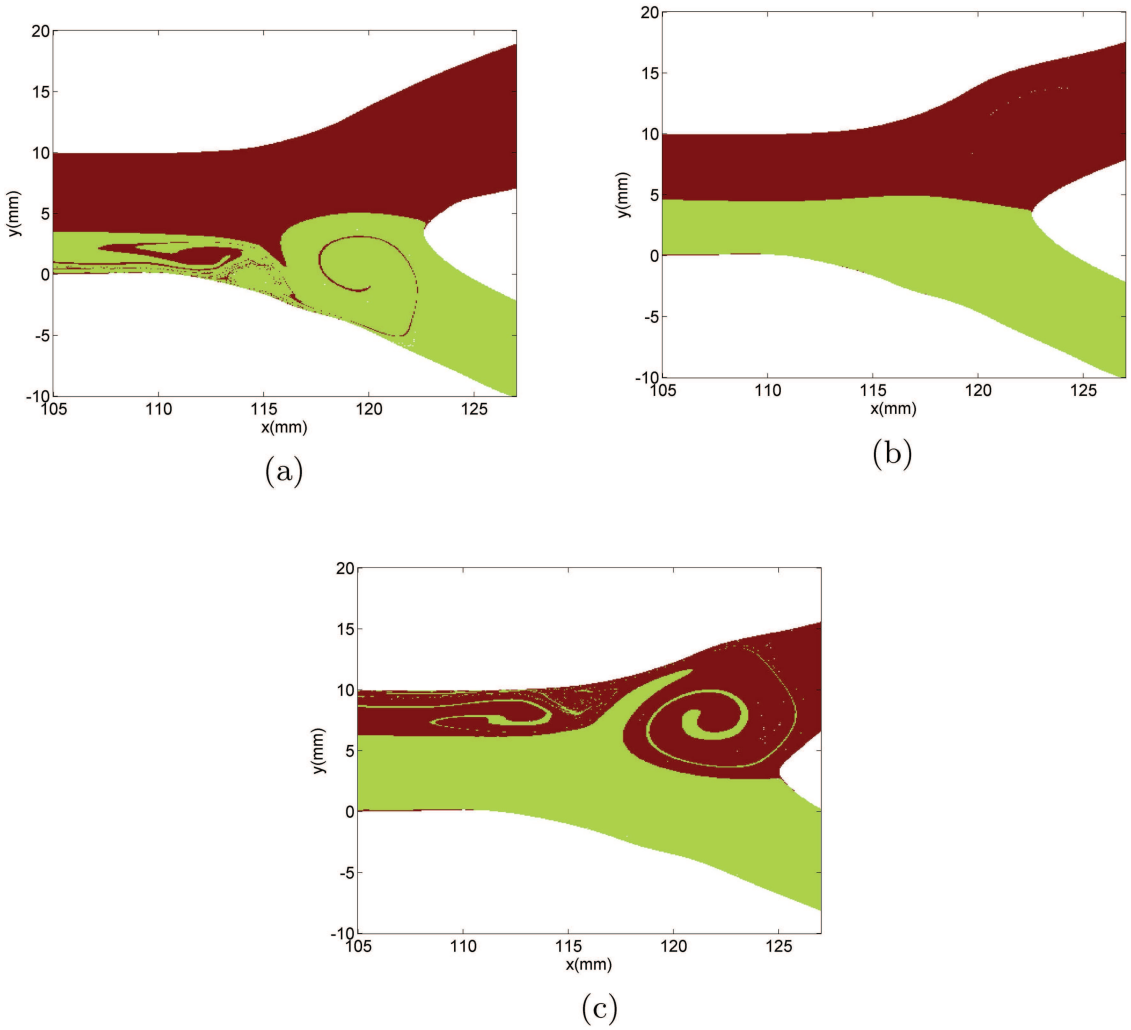

FIG. 5. Snapshot of the exit basin for each case at $t = 1/2T$. (a) Healthy case C1. (b) Mild stenosis C2. (c) Severe stenosis C3.

upper branch. To see how this distribution takes place, we calculate now the exit basin for each case.

C. Escape basins

Similar to the stable manifold, the exit basin is obtained by taking a 400×400 grid of initial points covering the bifurcation area. The trajectory of each initial condition is then traced and the branch through which the particle exits the system is then recorded. The initial points of particles leaving through the ICA (upper branch) are colored in dark red, while the ones that leave through the ECA (lower branch) are colored in green.

Figure 5 shows the results. For the healthy case, in Fig. 5(a), the exit basin shows that particles in the upper half of the artery leave the system through the upper branch, as the large red area indicates. This red basin also spreads to the lower half of the artery, with small filaments of particles that initially belong to the lower branch. Indeed, particles inside the lower branch can be captured by vortices, leaving after a while through upper branch.

The same is not true for the mild stenosis case, shown in Fig. 5(b). For this basin, there is a clear line dividing symmetrically the two basins. This symmetry is due the partial obstruction created by the stenosis, allowing the same amount of blood to flow through both branches.

As the obstruction further increases, the exit basins show an opposite behavior of particle capturing: all the particles in the lower half now leave the system through the same side, shown by the green basin in Fig. 5(c), and there are large green filaments reaching the upper half. Again, these filaments correspond to particles captured by re-circulation zones and exiting through the opposite side.

In order to quantify the escape basins, we compute now two quantities: the so-called basin entropy, a measurement that evaluates

TABLE II. Measurements of the escape basins: Basin boundary entropy and basin area.

	C1	C2	C3
S_B	0.9710	0.2979	1.5263
Area ICA	0.5723	0.4773	0.3387

the degree of mixing between different basins and the area of each basin.[32–34] The calculation of the basin entropy is performed by dividing the configuration space into N 2D boxes. The fraction of points leaving through each escape is then evaluated for each box through

$$p_I = \frac{n_I}{n_I + n_E}, \tag{5}$$

$$p_E = \frac{n_E}{n_I + n_E}, \tag{6}$$

where n_I is the number of particles escaping through the internal carotid artery and n_E is the number of particles escaping through the external carotid artery.

The entropy of each ith box is given by

$$S_i = -p_I \ln p_I - p_E \ln p_E. \tag{7}$$

The total basin entropy is then given by the average entropy of all boxes,

$$S_B = \frac{1}{N} \sum_{i=1}^{N} S_i. \tag{8}$$

The basin entropy measures the degree of uncertainty of a given exit basin.[32] For example, if we have a single exit basin then the probability of reaching it is equal to the unity and the basin entropy is equal to zero. On the other hand, if we have n_E so completely randomized exit basins that reaching each of them occurs with the same probability then the entropy is $\ln n_E$. Hence, $0 < S_b < \ln n_E$, in general.

Reducing the box size ε used to compute the probabilities, the number of boxes grows and also the entropy $S = \sum_{i=1}^{N_A}$ of each of the N boxes. However, the basin entropy $S_b = S/N$, in general, decreases with ε.

Let n_b be the number of boxes, which contain pieces of more than one exit basin, i.e., those boxes falling in the exit basin boundary. We then define the basin boundary entropy as $S_{bb} = S/n_b$. Since $N_b \leq N$, the maximum possible value of S_{bb} that a *smooth* (nonfractal) boundary can show is $\ln 2$. It has been argued that, if $S_{bb} > \ln 2$, then the exit basin boundary is fractal. Actually, this is a sufficient but not necessary condition, since there may be fractal exit boundaries with $S_{bb} < \ln 2$.

According to Table II, the cases C1 and C3 are thus characteristic of fractal exit basin boundaries, as already indicated by their box-counting dimension, whereas the case C2 has a smooth exit basin boundary. Moreover, according to the value of the basin boundary entropy, the final-state uncertainty related to the fractality of case C3 is higher than for C1.

TABLE III. Table of percentages of stenotic carotid occlusion.

Stenosis	x (mm)	y (mm)	y' (mm)	pre_{NA}	N_A
C2	4.40	10.94	9.96	59.8%	55.8%
C3	1.80	10.31	9.96	82.5%	81.9%

The so-called "basin stability parameter," which is the relative area of the exit basin, gives another quantitative measure of the final-state uncertainty related to the exit basin boundary structure.[35] In principle, the smaller is this area, the more unstable the final-state is with respect to small and arbitrary changes in the initial conditions. However, it is also important to take into account the topology of the basin boundary, since a fractal boundary of a basin of small area gives more final-state uncertainty than a smooth boundary of a basin with the same area. Hence, we should take those indicators as complementary. An example is provided by Table II, where the basin area is compared with the basin entropy: the former decreases as we go from C1 to C3, but in C2 the boundary is actually smoother than in C1 and C3. In this case, at least, the basin area gives a partially correct information on the final-state uncertainty.

IV. CONCLUSIONS

We studied particle advection in the carotid bifurcation for three different scenarios. The first case was considered to be a normal and healthy bifurcation, while the other two were affected by plaques in the internal carotid artery.

We showed that chaotic advection is prone to occur even for the healthy scenario. This might explain in part why the site is typically affected by circulatory diseases such as plaque formation and atherosclerosis.

The models of the carotid bifurcation with mild and severe stenosis showed that particle trapping is higher for the latter case. Also, for the severe stenosis, more particles leave the observation region through the ECA, the non-stenosed branch. This can result in the transportation of active particles, such as platelets, to other sites of the circulatory system.

As a next step, we plan to expand our model to a 3D version. We expect that the results will hold since they are related to a robust property of the flow: the symmetry induced by the stenosis.

SUPPLEMENTARY MATERIAL

See the supplementary material for a video tutorial of the flow computation in the carotid bifurcation with COMSOL Multiphysics.[28]

ACKNOWLEDGMENTS

This study was possible by partial financial support from the Brazilian agencies: FAPDF (No. 193.000.884/2015), National Council for Scientific and Technological Development (CNPq) (No. 407299/2018-1), and São Paulo Research Foundation (FAPESP) (No. 2018/03211-6).

TABLE IV. Eccentricity table and horizontal distance between stenotic carotids.

Stenosis	a (mm)	b (mm)	EI	Horizontal distance (mm)
C2	2.99	3.56	0.160	6.87
C3	3.89	4.61	0.156	4.33

APPENDIX: CLASSIFICATION OF THE STENOSIS

There are different methods in the literature to classify the degree of obstruction of a stenosis. Here, we use the NASCET criteria.[36] In this method, the percentage of the entrance of the occlusion, the pre-NASCET obstruction [Eq. (A1)], and the percentage of the stenosis as a whole, are given by

$$pre_{NA} = \frac{y - x}{y} 100\%, \tag{A1}$$

$$N_A = \frac{y' - x}{y'} 100\%, \tag{A2}$$

where x is the vertical space between the occlusions, y is the total carotid wall thickness inside the stenosis region, and y' is the carotid diameter after the stenosis, as shown in Fig. 1. The geometrical details and degree of obstruction of cases C2 and C3 are shown in Table III.

In general, plaques in blood vessels are not symmetrical and the characterization of such asymmetry is defined by the so-called eccentricity index (EI),

$$EI = \frac{b - a}{b}, \tag{A3}$$

where a and b are the maximum occlusion parameters. Table IV shows the geometrical parameters and the eccentricity index which is very close for both cases.

DATA AVAILABILITY

The data that support the findings of this study are available from the corresponding author upon reasonable request.

REFERENCES

[1] World Health Organization, "WHO—The top 10 causes of death" (2018).
[2] D. Liepsch, A. Balasso, H. Berger, and H. H. Eckstein, "How local hemodynamics at the carotid bifurcation influence the development of carotid plaques," Perspect. Med. **1-12**, 132–136 (2012).
[3] D. N. Ku, D. P. Giddens, C. K. Zarins, and S. Glagov, "Pulsatile flow and atherosclerosis in the human carotid bifurcation. Positive correlation between plaque location and low and oscillating shear stress," Arteriosclerosis 5, 293–302 (1985).
[4] M. Motomiya and T. Karino, "Flow patterns in the human carotid artery bifurcation," Stroke 15, 50–56 (1984).
[5] J. Vétel, A. Garon, and D. Pelletier, "Lagrangian coherent structures in the human carotid artery bifurcation," Exp. Fluids **46**, 1067–1079 (2009).
[6] R. Botnar, G. Rappitsch, M. B. Scheidegger, D. Liepsch, K. Perktold, and P. Boesiger, "Hemodynamics in the carotid artery bifurcation: A comparison between numerical simulations and in vitro MRI measurements," J Biomech. **33**, 137–144 (2000).
[7] H. Aref, "Stirring by chaotic advection," J. Fluid Mech. **143**, 1–21 (1984).
[8] T. Frommelt, M. Kostur, M. Wenzel-Schäfer, P. Talkner, P. Hänggi, and A. Wixforth, "Microfluidic mixing via acoustically driven chaotic advection," Phys. Rev. Lett. **100**, 1–4 (2008).
[9] G. Karolyi, A. Pentek, I. Scheuring, T. Tel, and Z. Toroczkai, "Chaotic flow: The physics of species coexistence," Proc. Natl. Acad. Sci. U.S.A. **97**, 13661–13665 (2000).
[10] K. V. Koshel' and S. V. Prants, "Chaotic advection in the ocean," Phys. Usp. **49**, 1151–1178 (2006).
[11] G. Károlyi and C. Grebogi, "Chaotic advection and fractality: Applications in oceanography," in *OCEANS 2007—Europe* (Aberdeen, 2007), pp.1–5.
[12] Y. Lou and F. Lutscher, "Evolution of dispersal in open advective environments," J. Math. Biol. **69**, 1319–1342 (2013).
[13] T. Tel, G. Karolyi, A. Pentek, I. Scheuring, Z. Toroczkai, C. Grebogi, and J. Kadtke, "Chaotic advection, diffusion, and reactions in open flows," Chaos **10**, 89–98 (2000).
[14] J. Ottino, "Mixing, chaotic advection, and turbulence," Annu. Rev. Fluid Mech. **22**, 207–253 (1990).
[15] T. Tél, A. de Moura, C. Grebogi, and G. Károlyi, "Chemical and biological activity in open flows: A dynamical system approach," Phys. Rep. **413**, 91–196 (2005).
[16] A. B. Schelin, G. Károlyi, A. P. De Moura, N. A. Booth, and C. Grebogi, "Chaotic advection in blood flow," Phys. Rev. E **80**, 1–7 (2009).
[17] A. B. Schelin, G. Károlyi, A. P. De Moura, N. A. Booth, and C. Grebogi, "Fractal structures in stenoses and aneurysms in blood vessels," Philos. Trans. R. Soc. A **368**, 5605–5617 (2010).
[18] A. B. Schelin, G. Károlyi, A. P. De Moura, N. Booth, and C. Grebogi, "Are the fractal skeletons the explanation for the narrowing of arteries due to cell trapping in a disturbed blood flow?," Comput. Biol. Med. **42**, 276–281 (2012).
[19] G. Závodszky, G. Károlyi, and G. Paál, "Emerging fractal patterns in a real 3D cerebral aneurysm," J. Theor. Biol. **368**, 95–101 (2015).
[20] S. C. Shadden, "Lagrangian coherent structures," in *Transport and Mixing in Laminar Flows*, edited by R. Grigoriev (Wiley, 2011).
[21] S. C. Shadden and A. Arzani, "Lagrangian postprocessing of computational hemodynamics," Ann. Biomed. Eng. **43**, 41–58 (2015).
[22] A. Arzani, S. C. Shadden, A. M. Gambaruto, and G. Chen, "Wall shear stress exposure time: A Lagrangian measure of near-wall stagnation and concentration in cardiovascular flows," Biomech. Model. Mechanobiol. **16**, 787–803 (2016).
[23] J. Toger, M. Kanski, M. Carlsson, S. Kovacs, G. Soderlind, H. Arheden, and E. Heiberg, "Vortex ring formation in the left ventricle of the heart: Analysis by 4D flow MRI and lagrangian coherent structures," Ann. Biomed. Eng. **40**, 2652–2662 (2012).
[24] S. C. Shadden and C. A. Taylor, "Characterization of coherent structures in the cardiovascular system," Ann. Biomed. Eng. **36**, 1152–1162 (2008).
[25] N. W. Bressloff, "Parametric geometry exploration of the human carotid artery bifurcation," J. Biomech. **40**, 2483–2491 (2007).
[26] B. Bharadvaj, R. Mabon, and D. Giddens, "Steady flow in a model of the human carotid bifurcation. Part II–laser-doppler anemometer measurements," J. Biomech. **15**, 363–378 (1982).
[27] R. F. Smith, B. K. Rutt, A. J. Fox, and R. N. Rankin, "Geometric characterization of stenosed human carotid arteries," Acad. Radiol. **3**, 898–911 (1996).
[28] COMSOL Multiphysicstextregistered v. 5.0.
[29] H. Kantz and P. Grassberger, "Repellers, semi-attractors, and long-lived chaotic transients," Physica D **17**, 75–86 (1985).
[30] T. Tél, M. Gruiz, K. Kulacsy, and S. Hadobas, *Chaotic Dynamics: An Introduction Based on Classical Mechanics* (Cambridge University Press, 2006).
[31] K. T. Alligood, T. D. Sauer, and J. A. Yorke, *Chaos: An Introduction to Dynamical Systems*, Textbooks in Mathematical Sciences (Springer, New York, 2000).
[32] A. Daza, A. Wagemakers, B. Georgeot, D. Guéry-Odelin, and M. A. F. Sanjuán, "Basin entropy: A new tool to analyze uncertainty in dynamical systems," Sci. Rep. **6**, 31416 (2016).
[33] A. Gusso, R. L. Viana, A. C. Mathias, and I. L. Caldas, "Nonlinear dynamics and chaos in micro/nanoelectromechanical beam resonators actuated by two-sided electrodes," Chaos Solitons Fractals **122**, 6–16 (2019).

[34]A. C. Mathias, R. L. Viana, T. Kroetz, and I. L. Caldas, "Fractal structures in the chaotic motion of charged particles in a magnetized plasma under the influence of drift waves," Physica A **469**, 681–694 (2017).
[35]P. J. Menck, J. Heitzig, N. Marwan, and J. Kurths, "How basin stability complements the linear-stability paradigm," Nat. Phys. **9**, 89–92 (2013).
[36]J. P. Archie, G. L. Moneta, J. M. Edwards, R. W. Chitwood, L. M. Taylor, R. W. Lee, and C. A. Cummings, "Correlation of north american symptomatic carotid endarterectomy trial (NASCET) angiographic definition of 70% to 99% internal carotid artery stenosis with duplex scanning," J. Vasc. Surg. **17**, 152–159 (1993).